Phys Chem Minerals (2013) 40:229–237
DOI 10.1007/s00269-013-0563-y

ORIGINAL PAPER

Synthesis and crystal structure of gold–silver sulfoselenides: morphotropy in the $Ag_3Au(Se,S)_2$ series

Yu. V. Seryotkin · G. A. Pal'yanova · V. V. Bakakin · K. A. Kokh

Received: 11 July 2012 / Accepted: 9 January 2013 / Published online: 1 February 2013

Abstract Gold–silver sulfoselenides of $Ag_3Au(Se,S)_2$ series—$Ag_3AuSe_{1.5}S_{0.5}$, Ag_3AuSeS, and $Ag_3AuSe_{0.5}S_{1.5}$—have been synthesized by fusing the elements in the required stoichiometric amounts in evacuated quartz ampoules. The single crystal X-ray diffraction data indicate the existence of two solid-solution series: petzite-type cubic Ag_3AuSe_2—Ag_3AuSeS (space group $I4_132$) and trigonal $Ag_3AuSe_{0.5}S_{1.5}$—Ag_3AuS_2 (space group $R\bar{3}c$). Both crystal structures differ in the distribution of Ag^+/Au^+ cations in the same distorted body-centered cubic sublattice of chalcogen anions. The morphotropic transformation results from the shrinkage of anion packing accompanied by the shortening of Ag–Ag distances. The structure of uytenbogaardtite mineral, earlier incorrectly interpreted as a tetragonal or cubic cell, is similar to that of the trigonal Ag_3AuS_2 end-member.

Keywords Gold–silver sulfoselenides · Crystal structure · Morphotropic transformation

Yu. V. Seryotkin · G. A. Pal'yanova · K. A. Kokh (✉)
Sobolev Institute of Geology and Mineralogy,
Siberian Branch of the RAS, prosp. Akad. Koptyuga 3,
630090 Novosibirsk, Russia
e-mail: k.a.kokh@gmail.com

Yu. V. Seryotkin
Novosibirsk State University, ul. Pirogova 2,
630090 Novosibirsk, Russia

V. V. Bakakin
Institute of Inorganic Chemistry, Siberian Branch of the RAS,
prosp. Lavrentieva 3, 630090 Novosibirsk, Russia

Introduction

Au–Ag chalcogenides—fischesserite (Ag_3AuSe_2) and uytenbogaardtite (Ag_3AuS_2)—are important concentrators of noble metals and tracer minerals of chalcogen fugacity in ore-forming processes. Since gold and silver chalcogenides are promising as narrow bandgap semiconductors (Yushko-Zakharova et al. 1986), it is necessary to develop methods for their production. These compounds are also of interest in the investigation of phase transformations in the Ag–Au–chalcogen system (Sakai et al. 1991). Admixtures of sulfur in fischesserite or selenium in uytenbogaardtite are a frequent phenomenon of anionic isomorphism in natural Au–Ag chalcogenides. (Botova et al. 1981; Greffie et al. 2002; Warmada et al. 2003; Savva and Pal'yanova 2007; Savva et al. 2010, 2012). The broad variations in S and Se concentrations in these minerals suggest the existence of isomorphic solid solution of the Ag_3AuS_2–Ag_3AuSe_2 series. Nekrasov et al. (1990) suggested the continuity of this series in the synthesized Ag–Au sulfoselenides. Messien et al. (1966) on the basis of an X-ray single-crystal experiment have reported the synthetic Ag_3AuS_2 to be a petzite-like cubic phase with $a = 9.72$ Å and space group $P4_132$. However, these data are not satisfactory in view of both the results of the structure refinement and its crystallographic characteristics. Graf (1968) described synthetic Ag_3AuS_2 phase as tetragonal with $a = 9.75$ Å and $c = 9.78$ Å according to the powder X-ray diffraction (XRD) data. The mineral uytenbogaardtite, Ag_3AuS_2, discovered by Barton et al. (1978) was also described as tetragonal (on the basis of powder diffraction data, $a = 9.68$–9.76 Å and $c = 9.78$–9.81 Å). Chen et al. (1979), and Wei (1981) revealed one more tetragonal polymorph of Ag_3AuS_2, liujinyinite ($a = 10.01$ Å and $c = 11.11$ Å). However, these data drop out of the series considering the density. Nekrasov et al. (1990)

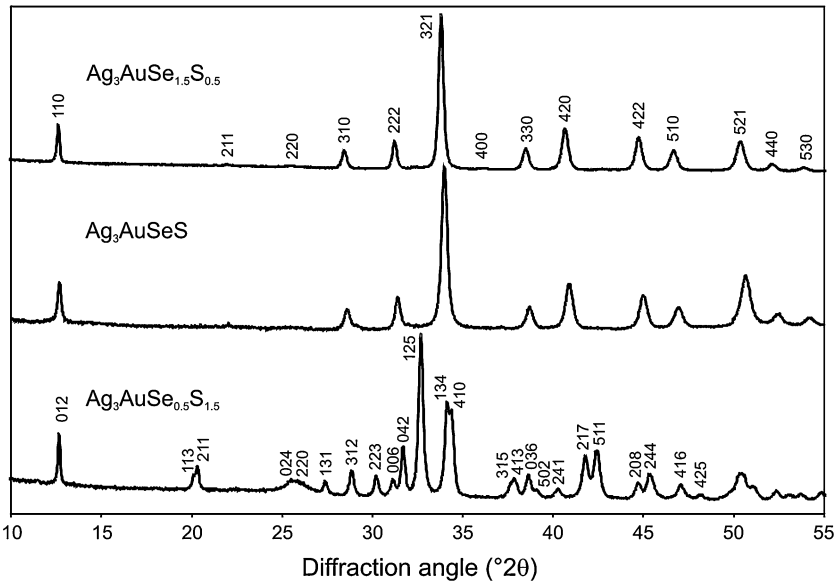

Fig. 1 Powder diffraction patterns of synthesized samples. Miller indices are given for cubic ($Ag_3AuSe_{1.5}S_{0.5}$) and trigonal ($Ag_3AuSe_{0.5}S_{1.5}$) lattices

report that the Ag_3AuS_2 phase is characterized by the cubic metrics of the unit cell ($a = 9.737$ Å). The authors have noted some extra lines uncommon for a cubic cell in their powder XRD patterns.

Recent single-crystal structure study (Seryotkin et al. 2011) of synthetic Ag_3AuS_2 has revealed a new structural type different from fischesserite, which casts further doubts on the continuity of the $Ag_3Au(Se,S)_2$ solid-solution series. The need for establishing and studying new gold–silver chalcogenides was noted by many authors (Bindi and Cipriani 2004; Nekrasov et al. 1990).

The aim of present study is to synthesize and study the structural properties of phases from the $Ag_3Au(Se,S)_2$ series and to critically analyze literature data.

Synthesis of gold–silver sulfoselenides

The dry synthesis of gold–silver chalcogenides generally involves heating of stoichiometric amounts of Ag^0 and Au^0 (or Ag–Au alloy) mixed with elemental selenium and/or sulfur. The heating performed in sealed evacuated ampoules is usually followed by annealing and cooling to ambient temperature (Smit et al. 1970; Wiegers 1976; Nekrasov et al. 1990; Sakai et al. 1991; Osadchii and Rappo 2004). Smit et al. (1970) have synthesized the Ag_3AuSe_2 compound by heating the corresponding Ag–Au–Se mixture up to 500 °C for 4 days and then slow cooling. Nekrasov et al. (1990) have synthesized Ag_3AuSe_2, Ag_3AuS_2, and other gold–silver sulfoselenides by fusing stoichiometric mixtures up to 700 °C for 4 days with the following annealing at 300 °C for 30 days and quenching in cold water. In case of visible inhomogeneities, the material synthesized was ground and fused again. Sakai et al. (1991) have also synthesized Ag_3AuSe_2 and Ag_3AuS_2 compounds at 700 °C but for the period of only 24 h (the annealing and cooling conditions have not been reported). Osadchii and Rappo (2004) performed the syntheses of Ag–Au–X (X = Se, S) samples in three successive steps at 450, 550, and 620 °C. After each step (10–12 days), intermediate homogenization in a mortar under acetone was carried out. The Au–Ag chalcogenides are known to be stable at room temperature and can transform to the high-temperature α-phases (Smit et al. 1970).

We have synthesized a number of phases in the pseudobinary Ag_3AuS_2—Ag_3AuSe_2 system. The end member of series—the Ag_3AuS_2 was synthesized and studied earlier (Seryotkin et al. 2011). Selenide fischesserite Ag_3AuSe_2 is well known also. Therefore, only intermediate compositions were studied. Mixtures of $Ag_3AuSe_{2-x}S_x$ composition (x = 0.5, 1.0, 1.5) produced from silver, gold (99.99 %), selenium, and sulfur (99.9 %) were weighed on the AG CH-8606 Greifensee-Zürich microbalance (Mettler Instruments; 0.05 mg precision). Each 500 mg sample was placed in a sealed evacuated quartz ampoule and heated up to 1,050 °C for 3 days at a rate of 0.2–0.5°/min. After 12 h at 1,050 °C, the ampoules were cooled to 500 °C at a rate of 0.2°/min and annealed at this temperature for 3 days. Then the furnace was turned off, and ambient temperature was achieved in about 7 h. The experimental products were examined using the X-ray powder diffraction and optical and electron microscopy. Chemical analyses of the synthesized phases and microcrystals were carried out on the MIRA LMU electron scanning microscopes (TESCAN) with the INCA Energy 350 + X-Max energy-dispersion spectrometer (Oxford Instruments). Operation conditions: accelerating voltage was 20 kV, probe current was 1 nA, spectrum recording during the analysis was 15 s.

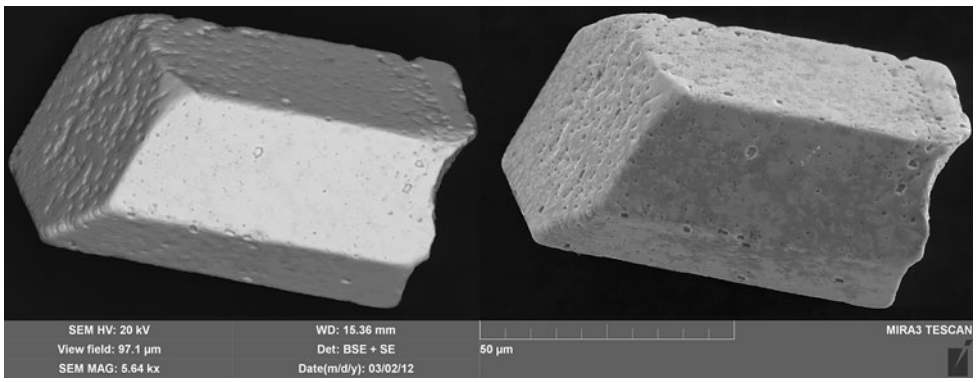

Fig. 2 The crystal of Au–Ag sulfoselenide of composition Ag_3AuSeS. Back-scattered electron and scattered electron images

Table 1 Crystallographic and experimental data for phases of $Ag_3Au(Se,S)_2$

	$Ag_3AuSe_{1.5}S_{0.5}$	Ag_3AuSeS	$Ag_3AuSe_{0.5}S_{1.5}$
a (Å)	9.92412(16)	9.86328(16)	13.7752(6)
c (Å)	–	–	17.2098(7)
V (Å^3)	977.41(3)	959.54(16)	2,828.2(3)
Z	8	8	24
Space group	$I4_132$	$I4_132$	R–3c
Crystal size (mm)	0.12 × 0.10 × 0.10	0.08 × 0.04 × 0.03	0.70 × 0.43 × 0.32
d (g/cm^3)	8.903	8.744	8.570
Diffractometer	Oxford diffraction xcalibur gemini R ultra		
Radiation	Mo Kα = 0.71,069 Å		
Scan type	ω	ω	ω
Scan width (deg/frame)	1	1	1
Exposure	45.00	46.91	24.67
2θ range (deg)	5.80–56.38	5.84–59.56	8.32–59.98
h_{min}, h_{max}; k_{min}, k_{max}; l_{min}, l_{max}	−12, 12; −12, 12; −13, 12	−13, 13; −13, 13; −13, 13	−16, 16; −16, 16; −20, 20
F(000)	2,232	2,160	6,264
μ (MoKα) (mm^{-1})	52.965	50.376	47.635
No. of I_{hkl} reflections measured	6,348	7,702	12,739
No. of unique F^2_{hkl}	207	235	561
R_{int}	0.0741	0.0510	0.0968
No. of observed reflections [$I > 2\sigma(I)$]	189	234	541
No. of variables	11	11	44
Flack *x* parameter	0.03(4)	0.09(4)	–
*R*1, *wR*2 for observed reflections [$I > 2\sigma(I)$]	0.0286, 0.0598	0.0350, 0.0624	0.0347, 0.0801
*R*1, *wR*2 for all data	0.0363, 0.0617	0.0350, 0.0624	0.0362, 0.0809
Residual electron density (*e*/Å^3)	1.034, −0.977	1.576, −1.419	1.943, −1.798

The samples were analyzed using Au $L_{\alpha 1}$, Ag $L_{\alpha 1}$, S $K_{\alpha 1}$, and Se $K_{\alpha 1}$. The accuracy of X-ray microprobe analysis was 0.5–1.5 rel. %. Pure metals (Au, Ag, and Se) and pyrite (FeS_2) were used as primary standards. Some microcrystals were investigated by means of single-crystal XRD.

All synthesized solid phases demonstrate optical homogeneity. According to the X-ray microprobe analysis, the compositions of the synthesized compounds can be represented as $Ag_3AuSe_{1.5}S_{0.5}$, Ag_3AuSeS, and $Ag_3AuSe_{0.5}S_{1.5}$, and the difference between analyses in different points being within the accuracy limit of the method. Sporadic semispheres of elemental selenium detected in some ampoules were probably formed from a gaseous phase.

X-ray powder diffraction study

The powder XRD data were obtained using the Thermo Scientific ARLX'TRA X-ray powder diffractometer equipped with a Peltier cooled Si(Li) solid-state detector

Table 2 Atomic coordinates, equivalent isotropic displacement parameters $U_{eq} = 1/3\ \Sigma_i\ (\Sigma_j\ (U_{ij}\ a_i^*\ a_j^*\ a_i\ a_j))$ ($Å^2$) and occupancies for phases of $Ag_3Au(Se,S)_2$

Atom	Multiplicity, site symmetry	Occupancy	*x*	*y*	*z*	U_{eq}
$Ag_3AuSe_{1.5}S_{0.5}$						
Ag	24 *f* 2..	1	0.37592(17)	0	0.25	0.0287(4)
Au	8 *a* .32	1	0.125	0.125	0.125	0.0252(3)
X	16 *e* .3.	$Se_{0.75}S_{0.25}$	0.26739(18)	0.26739(18)	0.26739(18)	0.0211(6)
Ag_3AuSeS						
Ag	24 *f* 2..	1	0.37900(17)	0	0.25	0.0275(3)
Au	8 *a* .32	1	0.125	0.125	0.125	0.0212(3)
X	16 *e* .3.	$Se_{0.5}S_{0.5}$	0.26734(19)	0.26734(19)	0.26734(19)	0.0198(6)
$Ag_3AuSe_{0.5}S_{1.5}$						
Ag1	36 *f* 1	1	0.04804(10)	0.21757(10)	0.33670(7)	0.0204(4)
Ag2	36 *f* 1	0.96	−0.1633(2)	0.04136(14)	0.42369(14)	0.0471(6)
Au1	6 *a* 32	1	0	0	0.25	0.0127(4)
Au2	18 *e* .2	1	−0.24654(6)	0	0.25	0.0124(3)
Au3	36 *f* 1	0.040(4)	−0.1298(15)	0.0396(16)	0.4580(13)	0.022(7)*
X1	12 *c* 3.	$Se_{0.25}S_{0.75}$	0	0	0.3890(2)	0.0112(9)
X2	36 *f* 1	$Se_{0.25}S_{0.75}$	−0.1534(2)	0.1825(2)	0.30348(15)	0.0171(6)

* Au3 position was refined isotropically

Table 3 Atomic displacement parameters (Å) for phases of $Ag_3Au(Se,S)_2$

Atom	U_{11}	U_{22}	U_{33}	U_{12}	U_{13}	U_{23}
$Ag_3AuSe_{1.5}S_{0.5}$						
Ag	0.0365(9)	0.0253(9)	0.0243(9)	0	0	0.0016(6)
Au	0.0252(3)	0.0252(3)	0.0252(3)	0.0012(4)	0.0012(4)	0.0012(4)
X	0.0211(6)	0.0211(6)	0.0211(6)	0.0032(7)	0.0032(7)	0.0032(7)
Ag_3AuSeS						
Ag	0.0367(8)	0.0225(7)	0.0234(7)	0	0	0.0027(5)
Au	0.0212(3)	0.0212(3)	0.0212(3)	0.0016(3)	0.0016(3)	0.0016(3)
X	0.0198(6)	0.0198(6)	0.0198(6)	0.0042(7)	0.0042(7)	0.0042(7)
$Ag_3AuSe_{0.5}S_{1.5}$						
Ag1	0.0184(6)	0.0208(6)	0.0214(6)	0.0093(5)	−0.0011(5)	−0.0047(5)
Ag2	0.0791(14)	0.0308(9)	0.0351(10)	0.0302(9)	0.0280(11)	0.0060(7)
Au1	0.0121(5)	0.0121(5)	0.0140(7)	0.0060(2)	0	0
Au2	0.0138(4)	0.0132(5)	0.0101(4)	0.0066(2)	0.00,114(14)	0.0023(3)
X1	0.0122(13)	0.0122(13)	0.0093(19)	0.0061(7)	0	0
X2	0.0198(14)	0.0194(14)	0.0147(12)	0.0118(12)	−0.0015(11)	−0.0015(11)

(Cu$K\alpha$ radiation). A step-scan mode data collection was employed using a step size of 0.02° and a 10 s count time per step. The 2θ range was 8–60°. The results were processed with the WinXRD 2.0–6 (Thermo Scientific). The comparison of experimental and calculated diffraction patterns carried out using PowderCell 2.4 program (Kraus and Nolze 1996). Diffraction patterns of synthesized samples are shown in Fig. 1. All peaks on the diffraction pattern of $Ag_3AuSe_{0.5}S_{1.5}$ are indicated in trigonal unit cell, whereas diffraction patterns of Ag_3AuSeS and $Ag_3AuSe_{1.5}S_{0.5}$ belong to cubic petzite-like phases. Therefore, the results of powder XRD confirm the conclusion about the homogeneity of synthesized samples.

Single-crystal X-ray diffraction study

The crystals of $Ag_3AuSe_{1.5}S_{0.5}$, Ag_3AuSeS, and $Ag_3AuSe_{0.5}S_{1.5}$ phases were selected for single-crystal XRD experiments on the Oxford Diffraction Gemini R Ultra diffractometer

Table 4 Interatomic distances (Å) and X–Ag(Au)–X angles (°) in the phases of $Ag_3Au(Se,S)_2$

	$Ag_3AuSe_{1.5}S_{0.5}$	Ag_3AuSeS	
Ag–X(2×)	2.7074(10)	2.6753(10)	
Ag–X(2×)	2.8691(13)	2.8627(13)	
X–Ag–X(2×)	94.84(7)	94.94(7)	
X–Ag–X(2×)	107.75(6)	107.84(7)	
X–Ag–X	117.53(11)	118.67(12)	
X–Ag–X	135.90(11)	134.74(12)	
Au–X(2×)	2.448(3)	2.432(3)	
X–Au–X	180	180	
Au–Ag(6×)	3.0461(14)	3.0523(14)	
Ag–Ag(2×)	3.0312(14)	2.9881(13)	
Ag–Ag(2×)	3.0461(14)	3.0526(14)	
$Ag_3AuSe_{0.5}S_{1.5}$			
Au1–X1(2×)	2.393(4)	Au1–Ag1(6×)	3.1086(12)
X1–Au1–X1	180		
		Au2–Ag1(2×)	2.9112(12)
Au2–X2(2×)	2.363(3)	Au2–Ag1(2×)	2.9616(12)
X2–Au2–X2	178.71(14)	Au2–Ag2(2×)	3.150(3)
Au3–X1	2.425(18)	Au3–Ag2	3.08(2)
Au3–X2	2.431(19)	Au3–Ag2	3.18(2)
Au3–X2	2.708(19)	Au3–Ag1	3.22(2)
X1–Au3–X2	145.3(8)	Au3–Ag1	3.26(2)
X2–Au3–X2	105.1(7)	[Au3–Ag2]	0.76(2)
		[Au3–Au3(2×)]	2.56(3)
Ag1–X2	2.630(3)	Ag1–Ag2	3.011(2)
Ag1–X2	2.859(3)	Ag1–Ag2	3.089(2)
Ag1–X2	2.866(3)	Ag1–Ag1	3.197(2)
Ag1–X1	2.8720(18)	Ag1–Ag1	3.232(2)
X1–Ag1–X2	93.98(9)		
X2–Ag1–X2	96.28(10)		
X1–Ag1–X2	101.82(7)		
X2–Ag1–X2	111.28(7)		
X2–Ag1–X2	126.81(9)		
X1–Ag1–X2	130.10(10)		
Ag2–X2	2.586(3)	Ag2–Ag2	3.080(5)
Ag2–X2	2.620(3)		
Ag2–X1	2.650(3)		
Ag2–X2	2.795(4)		
X2–Ag2–X2	92.70(11)		
X2–Ag2–X2	103.31(6)		
X1–Ag2–X2	103.38(11)		
X1–Ag2–X2	105.36(9)		
X1–Ag2–X2	124.63(15)		
X2–Ag2–X2	129.82(14)		

(CCD detector, graphite-monochromatized Mo$K\alpha$ radiation). During processing of data performed with CrysAlisPro software, the space groups for $Ag_3AuSe_{1.5}S_{0.5}$ ($I4_132$) and $Ag_3AuSe_{0.5}S_{1.5}$ ($R\bar{3}c$) were selected on the basis of reflection intensities and systematic absences. The $Ag_3AuSe_{1.5}S_{0.5}$ phase is identical to mineral fischesserite (Bindi and Cipriani 2004), while the $Ag_3AuSe_{0.5}S_{1.5}$ phase demonstrates similarity to the Ag_3AuS_2 phase studied earlier (Seryotkin et al. 2011).

Some problems arose when determining the space group for the Ag_3AuSeS phase (Fig. 2). Though the diffraction pattern may be described generally by the $I4_132$ space group, some reflections forbidden for a body-centered cell were observed. The refinement of structure in a triclinic symmetry was unsuccessful: the most discrepant reflections are found to be forbidden in the body-centered cell. Thus, the experimental data were processed in the $I4_132$ space group. The nature of forbidden reflections will be discussed below. The structure determinations were performed using the SHELX software (Sheldrick 2008). The details of data collection and structure determinations are shown in Table 1. Refined atomic coordinates and displacement parameters are given in Tables 2 and 3, respectively. No evidence of any Se/S ordering has been observed. The selected interatomic distances and angles are listed in Table 4. All structural data have been deposited as CIFs in the ICSD (CSD-nos. 424422–424424).

Results and discussion

The known structures of Ag_3AuX_2 phases (X = S, Se, Te) demonstrate some similarity: their anionic subsystem is a slightly distorted body-centered cubic packing. Such a subsystem may be entirely divided into distorted tetrahedra or sphenoids (Seryotkin et al. 2011). The formula unit contains twelve sphenoids, a quarter of which are occupied by Ag atoms. The edges shared by four vacant sphenoids are occupied by Au atoms.

The structures of Ag_3AuX_2 chalcogenides may be described on the basis of infinite rods situated along threefold axes (Fig. 3). These rods, joined by the shared edges of Ag-sphenoids, are multiplied by base translations of cubic (rhombohedric) unit cell. The building unit of the rod, $Ag_{12}Au_4X_{20}$, consists of four X–Au–X linear groups (one of them lies on the rod axis) and 2 × 6 Ag-tetrahedra around the axial X atoms (Fig. 4). The building units are joined with each other via six X anions. Two ways of this joining may be observed: by the shared edges (cubic structure, Fig. 4) or by the shared vertices of Ag tetrahedra (trigonal structure, Fig. 4).

The unit cell linear parameters and the volume of synthesized phases increase linearly with the amount of selenium in formula (Fig. 5). Morphotropic transformation appears only as an abrupt increase in the α angle from 89.2° to 90.0° (Fig. 5). Such a minor difference between cubic and trigonal (rhombohedral) cell is due to the

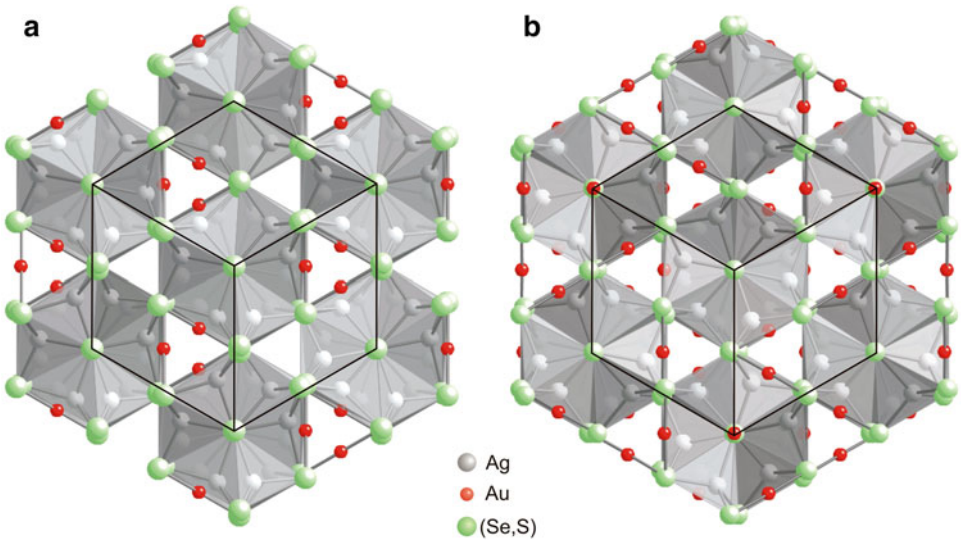

Fig. 3 The Ag_3AuX_2 cubic (**a**) and trigonal (**b**) structures (view along threefold axis). The $(Ag_{12}Au_4X_{14})^{\infty}$ rods are multiplied by basic translations and joined with each other by shared edges of Ag-tetrahedra

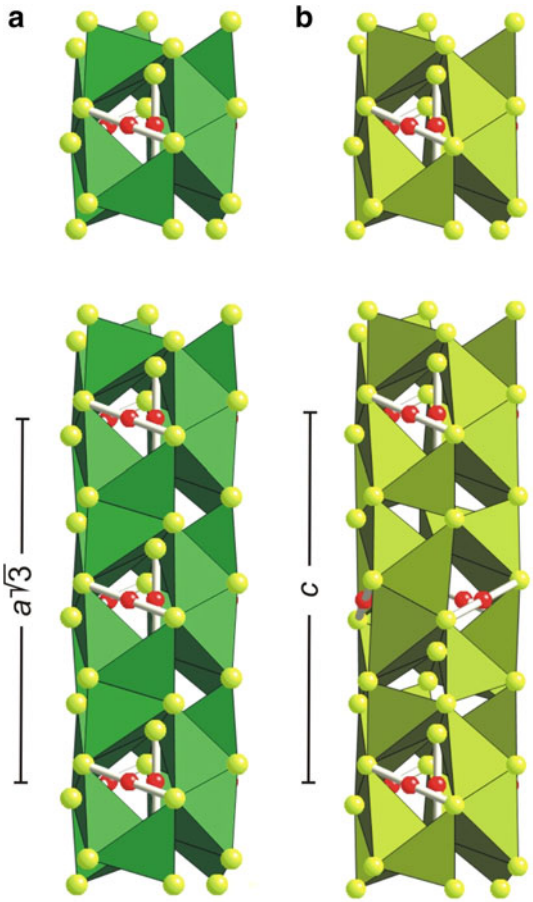

Fig. 4 The $Ag_{12}Au_4X_{20}$ building units (*top*) and their joining into rods along threefold axis in the case of cubic (**a**) and trigonal (**b**) structures

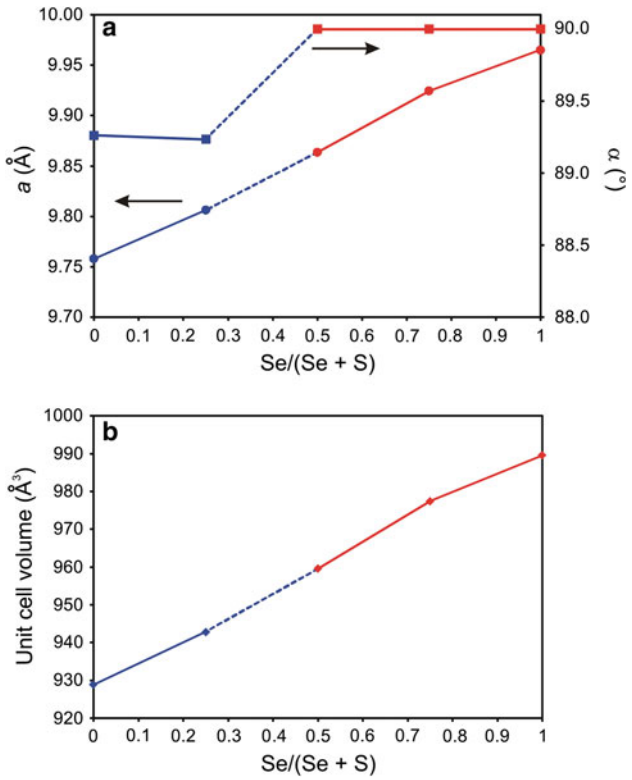

Fig. 5 Variation of unit cell metrics in the Ag_3AuSe_2—Ag_3AuS_2 series. Data for end-members selenide fischesserite Ag_3AuSe_2 and sulfide Ag_3AuS_2 are given from Bindi and Cipriani (2004) and Seryotkin et al. (2011) respectively

common body-centered chalcogen subsystem, which is retained over the whole range of chemical compositions under study. However, the cation distribution is different for cubic and trigonal phases. In the cubic (petzite-type) structure, all Ag-tetrahedra are equivalent and have four shared edges each, thus yielding four short Ag–Ag distances (Table 4). The trigonal structure includes two types of Ag-tetrahedra, the first having four shared edges and the second having three. The fourth Ag atom shifted from the neighbor Ag atom for more than 0.5 Å and retained only one shared O atom.

Table 5 Comparison of crystal structures of Ag_3AuX_2 (X = Te, Se, (Se,S), S)

	Ag_3AuTe_2 petzite [1]	Ag_3AuSe_2 fischesserite [2]	$Ag_3Au(Se_{1.5}S_{0.5})$ [3]	Ag_3AuSeS [3]	$Ag_3Au(Se_{0.5}S_{1.5})$ [3]	Ag_3AuS_2 [4]	Ag_3AuS_2 (simulated) [3]
Symmetry	cub. $I4_132$	cub. $I4_132$	cub. $I4_132$	cub. $I4_132$	trig. $R\bar{3}c$	trig. $R\bar{3}c$	cub. $I4_132$
a (Å)	10.385	9.965	9.924	9.863	9.806	9.758	9.758
α (deg.)					89.24	89.26	
$V_{u.c.}$ (Å^3)	1,120.0	989.5	977.41	959.54	942.74	928.80	929.1
X–Au–X	5.22	5.20	4.90	4.86	4.79	4.69	4.63
X···X (Å)	3.78	3.43	3.69	3.68	3.82	3.87	3.82
					4.73 (3×)	4.66 (3×)	
					4.08 (3×)	4.08 (3×)	
Ag–X (4×)	2.91–2.97	2.78–2.89	2.71–2.87	2.68–2.86	2.59–2.87	2.57–2.86	2.65–2.82
Average	2.94	2.83	2.79	2.77	2.735	2.724	2.74
Au–Ag (6×)	3.06	2.95	3.05	3.05	3.11	3.10	3.05
Ag–Ag	3.07–3.30	2.95–3.16	3.03–3.05	2.99–3.05	3.01–3.23	3.01–3.24	2.93–3.05
Average	3.18	3.05	3.04	3.02	3.12	3.12	2.99

[1] Chamid et al. (1978), [2] Bindi and Cipriani (2004), [3] this work, [4] Seryotkin et al. (2011)

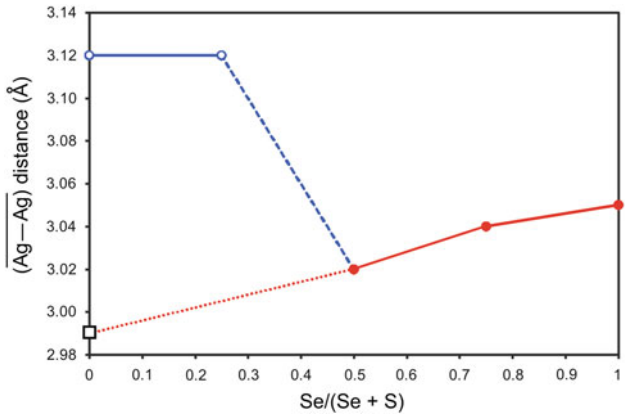

Fig. 6 Mean Ag–Ag distances in cubic (*filled circles*) and trigonal (*open circles*) Ag_3AuX_2 structures. Data for end-members selenide fischesserite Ag_3AuSe_2 and sulfide Ag_3AuS_2 are given from Bindi and Cipriani (2004) and Seryotkin et al. (2011) respectively. *Square* corresponds to the model cubic Ag_3AuS_2 structure

When the mean size of X anion decreases, the petzite-type cubic structure shrinks. Therefore, the mean Ag–X distances and the lengths of X–Au–X linear groups shorten (Table 5). The Ag–Au distances at that virtually do not change, and the major changes occur in the net of the Ag atoms. Thus, the mean Ag–Ag distance decreases from 3.18 Å in petzite (Ag_3AuTe_2) to 3.02 Å in Ag_3AuSeS (Table 5). An increase in sulfur content at the same structure type would lead to further shortening of Ag–Ag distances down to 2.93–3.05 Å (2.99 Å on the average) in the model petzite-like Ag_3AuS_2 structure (Table 5; Fig. 6). It is generally assumed that the Ag–Ag interactions help to stabilize the structures of Ag chalcogenides. However, the stabilizing effect of such interaction is limited to a certain range of interatomic distances. While redundant shortening may cause instability of the crystal structure. Since the Ag–Ag distance is equal to 2.89 Å in metal silver (Spreadborough and Christian 1959), it can be assumed that the approach to this value is critical. Probably the same interaction causing destabilization of petzite-like crystal structure causes the morphotropic transformation.

The resulting modification is characterized by substantially increased Ag–Ag distances, which are virtually independent of the Se/S ratio.

Taking into account the crystal ionic radii of Te^{2-} and Se^{2-} (2.07–1.84 Å, Shannon, 1981), X–X distances in petzite (Chamid et al. 1978) and fischesserite (Bindi and Cipriani 2004) structures are abnormally short (Table 5). This can be interpreted as expressing covalency trend of anion–anion interaction (Makovicky 2006). An increase in sulfur share in sample composition decreases the above-mentioned differences and promotes (due to scale shrinkage of structure) cation–cation interaction.

The above-mentioned occurrence of reflections forbidden for a body-centered cell in the diffraction pattern of Ag_3AuSeS crystal may be interpreted as follows. A small amount of the trigonal Ag_3AuX_2 phase with space group $R\bar{3}c$ is present in the investigated sample as a result of the intergrowth process. This maybe possible due to the same geometry of anion subsystem (body-centered pseudocubic with a parameter of 4.04–4.27 Å) for both structure types. The observed intensities of additional reflections were compared with calculated ones, which showed that the concentration of trigonal phase was about 1 %. Thus, the composition limit of the cubic phase stability is situated

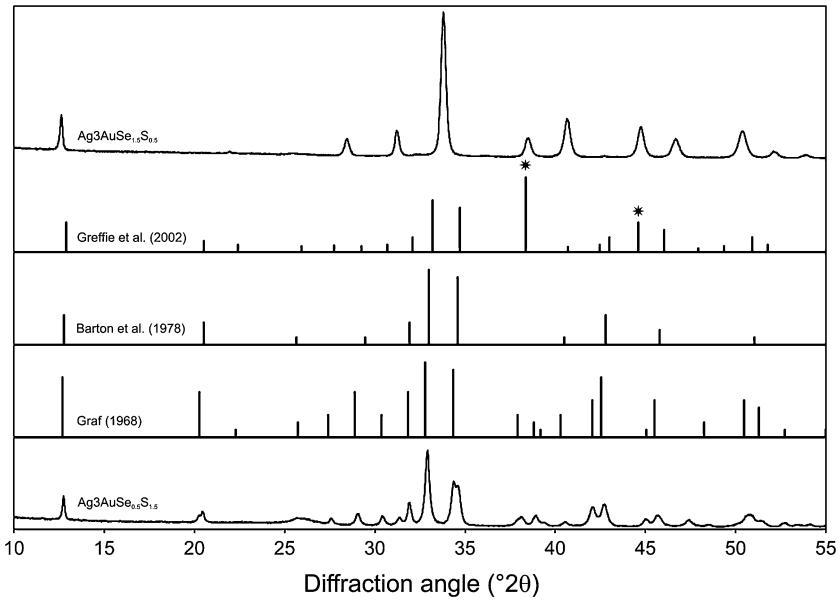

Fig. 7 The comparison of powder XRD patterns of uytenbogaardtite (Barton et al. 1978; Greffie et al. 2002) and its synthetic analog (Graf 1968) with diffraction profiles for cubic petzite-like $Ag_3AuSe_{1.5}S_{0.5}$ phase (*top*) and trigonal $Ag_3AuSe_{0.5}S_{1.5}$ (*bottom*). *Asterisks* indicates *diffraction lines* of (Ag,Au) phase

close to Ag_3AuSeS. Since at the ratio of 1/3 only a trigonal phase is stable, its stability limit lies in the $1/3 \leq Se/S < 1/1$ range, which will be the object of further research.

The low-occupated Au3 position alternative with Ag2 site is fixed in $Ag_3AuSe_{0.5}S_{1.5}$ structure (Table 2). Remarkably that the same position with closed population was localized in structure of sulfide Ag_3AuS_2 (Seryotkin et al. 2011). Reasons of their presences are unclear. It can be assumed that these samples contain an impurity phase $(Ag,Au)_2S$ with the same pseudocubic body-centered anion matrix. As we have mentioned earlier (Seryotkin et al. 2011) that the continuity in Ag_3AuSe_2–Ag_3AuS_2 series declared by Nekrasov et al. (1990) can exist if the end-members are of the same structure type. It is worth noting that the conclusion of Nekrasov et al. (1990) was based on the powder XRD data, which showed a linear increase in the pseudocubic *a*-parameter with the increase of Se/(Se + S) ratio. In fact, our results confirm the linear dependence (Fig. 4) but does not imply the structure identity throughout the investigated range. As we have shown above, the morphotropic transformation in the Ag_3AuSe_2–Ag_3AuS_2 system affects not only the symmetry, but the structure type as well. However, the *a*-parameter and unit cell volume demonstrate no discontinuity (Fig. 5).

Mineral uytenbogaardtite Ag_3AuS_2 discovered by Barton et al. (1978), along with its synthetic analogue, investigated by Graf (1968), was described as a tetragonal phase with a space group $P4_122$ or $P4_1$. The structure of uytenbogaardtite has not been correctly determined yet. The data on the cubic structure of this phase (Messien et al. 1966) seem to be not valid to date. Figure 7 demonstrates the experimental powder XRD patterns of uytenbogaardtite (Barton et al. 1978; Greffie et al. 2002) and synthetic Ag_3AuS_2 (Graf 1968) compared with the powder patterns of cubic petzite-like Ag_3AuSeS phase (top) and trigonal $Ag_3AuSe_{0.5}S_{1.5}$ modification (bottom). The differences between the uytenbogaardtite data and the diffraction profile of the cubic phase are clearly seen. At the same time, there is appreciable similarity between uytenbogaardtite and trigonal phase powder patterns concerning both the intensities and the positions of reflections. Thus, it can be stated with certain confidence that the choice of the tetragonal symmetry for synthetic Ag_3AuS_2 by Graf (1968) and for uytenbogaardtite by Barton et al. (1978) was incorrect. Corresponding powder XRD patterns maybe indexed in a trigonal (rhombohedral) cell with $a \approx 9.76$ Å and $\alpha \approx 89.3°$. Thus, the structure of uytenbogaardtite is identical to that of synthetic Ag_3AuS_2, which we have described earlier (Seryotkin et al. 2011).

Acknowledgments We wish to thank Jiri Sejkora and Emil Makovicky for their reviews that helped us to clarify the presentation of this paper. This work was supported by the Russian Foundation for Basic Research (Grant 11-05-00504a).

References

Barton MD, Kieft C, Burke EAJ, Oen IS (1978) Uytenbogaardtitae, a new silver-gold sulfide. Can Miner 16:651–657

Bindi L, Cipriani C (2004) Structural and physical properties of fischesserite, a rare Gold–silver selernide from the de Lanar Mine, Owyhee County, Idaho, USA. Can Miner 42:1733–1737. doi:10.2113/gscanmin.42.6.1733

Botova MM, Bergman YuS, Balyasnikov AA, Sandomirskaya SM, Chuvikina NG (1981) 1st occurrence of fischesserite in the USSR. Dokl Akad Nauk SSSR 256:1465–1469

Chamid S, Pobedimskaya EA, Spiridonov EM, Belov NV (1978) Refinement of the structure of petzite, $AuAg_3Te_2$. Kristallografiya 23:483–486

Chen Z, Guo Y, Zen J, Xu W (1979) On discovery and investigation of liujinyinite. Kexue Tongbao 24:843–848

Graf RB (1968) The system Ag_3AuS_2–Ag_2S. Am Miner 53:496–500

Greffie C, Bailly L, Milési J-P (2002) Supergene alteration of primary ore assemblages from low-sulfidation Au–Ag epithermal deposits at Pongkor, Indonesia, and Nazareno, Peru. Econ Geol 97:561–571. doi:10.2113/97.3.561

Kraus W, Nolze G (1996) POWDER CELL—a program for the representation and manipulation of crystal structures and calculation of the resulting X-ray powder patterns. J Appl Cryst 29:301–303. doi:10.1107/S0021889895014920

Makovicky E (2006) Crystal structure of sulphides and other chalcogenides. Rev Mineral Geochem 61(1):7–125. doi:10.2138/rmg.2006.61.2

Messien P, Baiwir M, Tavernier B (1966) Structure cruistalline du sulfure mixte d'argent et d'or. Bull Soc R Sci Liege 35:727–733

Nekrasov IYa, Lunin SE, Egorova NV (1990) X-Ray diffraction study of the Ag–Au–S–Se system compounds. Dokl Akad Nauk SSSR 311:943–946

Osadchii EG, Rappo OA (2004) Determination of standard thermodynamic properties of sulfides in the Ag–Au–S system by means of a solid-state galvanic cell. Amer Miner 89:1405–1410

Sakai H, Ando M, Ichiba S, Maeda Yu (1991) Au-197 Mossbauer spectroscopic study of the ternary-systems (Ag, Au)2X (X = S and Se). Chem Lett 20:223–226. doi:10.1246/cl.1991.223

Savva NE, Pal'yanova GA (2007) Genesis of gold and silver sulfides at the Ulakhan deposit (northeastern Russia). Rus Geol Geoph 48:799–810. doi:10.1016/j.rgg.2007.09.006

Savva NE, Pal'yanova GA, Kolova EE (2010) Gold and silver minerals in zone of secondary sulfide concentration (Krutoe ore occurrence, northeastern Russia). Vestnik SVNTs DVO RAN 1:33–45

Savva NE, Pal'yanova GA, Byankin MA (2012) The problem of genesis of gold and silver sulfides and selenides in the Kupol deposit (Chukotka, Russia). Rus Geol Geoph 53:457–466. doi:10.1016/j.rgg.2012.03.006

Seryotkin YuV, Bakakin VV, Pal'yanova GA, Kokh KA (2011) Synthesis and crystal structure of the trigonal silver(I) dithioaurate(I), Ag_3AuS_2. Cryst Growth Des 11:1062–1066. doi:10.1021/cg1012318

Shannon RD (1981) Bond distances in sulfides and a preliminary table of sulfide crystal radii. In: O'Keefe M, Navrotsky A (eds) Structure and bonding in crystals, vol II. Academic Press, New York, pp 53–70

Sheldrick GM (2008) A short history of SHELX. Acta Crystallogr A64:112–122. doi:10.1107/S0108767307043930

Smit TJM, Venema E, Wiersma J, Wiegers GA (1970) Phase transitions in silver gold chalcogenides. J Solid State Chem 2:309–312

Spreadborough J, Christian JW (1959) High-temperature X-ray diffractometer. J Sci Instrum 36:116–118

Warmada IW, Lehmann B, Simandjuntak M (2003) Polymetallic sulfides and sulfosalts of the pongkor epithermal Gold–silver deposit, West Java, Indonesia. Can Miner 41:185–200. doi:10.2113/gscanmin.41.1.185

Wei M (1981) Some new data on the crystal structure of liujinyinite. Sci Geolo Sin 3:232–234

Wiegers GA (1976) Electronic and ionic conduction of solid solutions $Ag_{2-x}Au_xSe$ ($0 \leq x \leq 0.5$). J Less-Common Metals 48:269–283

Yushko-Zakharova OE, Ivanov VV, Soboleva LN, Dubakina LS, Sherbachev DK, Kulishichina RD, Timofeev OS (1986) Minerals of noble metals. Nedra, Moscow